Ph-X Bond Activation
Grand Prix
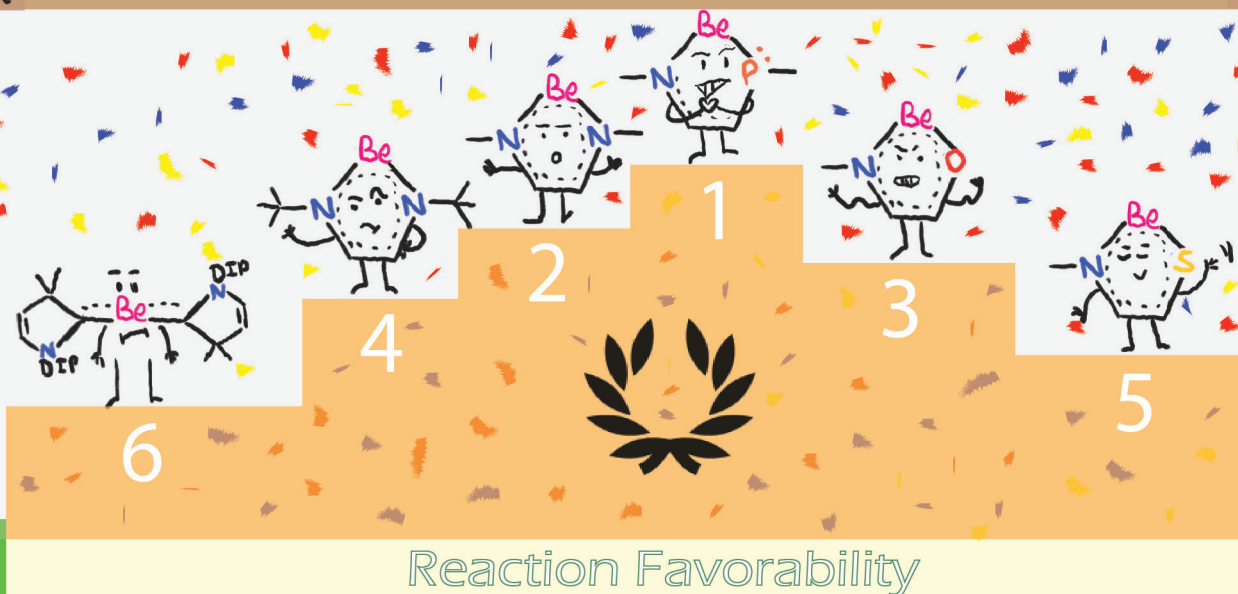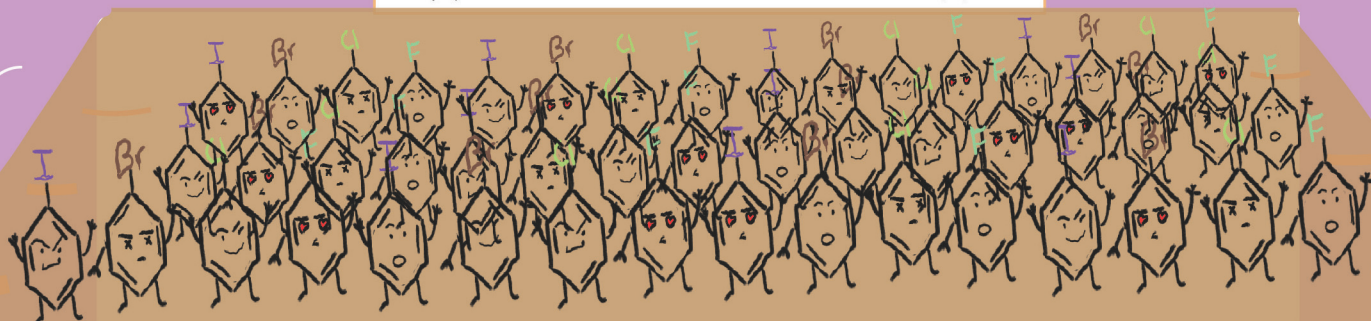
Reaction Favorability

ROYAL SOCIETY
OF CHEMISTRY

PAPER
J. Oscar C. Jiménez-Halla, Miquel Solà *et al.*
Beryllium compounds for the carbon–halogen bond
activation of phenyl halides: the role of non-innocent ligands

PAPER

Beryllium compounds for the carbon–halogen bond activation of phenyl halides: the role of non-innocent ligands†

Daniel E. Trujillo-González, [ID] [a,b] Gerardo González-García, [ID] [a] J. Oscar C. Jiménez-Halla*[a] and Miquel Solà [ID] *[b]

Beryllium is a metallomimetic main-group element, *i.e.*, it behaves similarly to transition metals (TMs) in some bond activation processes. To investigate the ability of Be compounds to activate C–X bonds (X = F–I), we have computationally investigated, using DFT methods, the reaction of **(CAAC)₂Be** (CAAC = 1-(2,6-diisopropylphenyl)-3,3,5,5-tetramethylpyrrolidin-2-ylidene) and a series of five-membered hetero-cyclic beryllium bidentate ligands with phenyl halides. We have analysed all plausible reaction mechanisms and our results show that, after the initial C–X oxidative addition, migration of the phenyl group occurs towards the less electronegative heteroatom. Our theoretical study highlights the important role of biden-tate non-innocent ligands in providing the required electrons for the initial Ph–X oxidative addition. In contrast, the monodentate ligand, CAAC, does not favour this oxidative addition.

Introduction

In the last decade, advancement of s- and p-block chemistry has taken place as a consequence of the potential of some of these elements to replicate the behaviour of transition metals (TMs) in catalysis, the so-called metallomimetic chemistry.[1] In the last few years, we have witnessed several studies reporting on the ability of the main-group elements to activate C–H and H–H bonds[2–4] among others. Alkaline-earth metals (usually Mg, Ca, Sr, and Ba compounds) have been shown to carry out hydroamination, heterofunctionalization, and cross-meta-thesis reactions,[5] which were only attributed to TMs in the past. Among these elements, beryllium is less preferred to be explored experimentally since it is toxic to human health (long-term exposure causes berylliosis).[6–9] However, nowadays it is possible to develop beryllium chemistry with appropriate safety conditions.[8]

Despite its toxicity, beryllium and its compounds have caught the attention of researchers in the last decades due to their applications in materials science and nuclear physics.[6,7,10] However, until 2015, less than 180 beryllium com-pounds, which contain Be–N, Be–C and Be–P bonds, were reported according to the Cambridge structural database.[11]

Beryllium dihalides form stable complexes with Lewis bases.[12–14] Thus, different ligands are used to stabilize the empty orbitals of the beryllium atom. For instance, Frenking and coworkers analyzed a tetracoordinate beryllium compound that was synthesized by the reaction between BeCl₂ and two molecules of bis(diphenylphosphino)methane in dichloro-methane (Chart 1a).[15] Using toluene as a solvent, Petz and coworkers reported a tricoordinate beryllium compound obtained from the reaction between BeCl₂ and C(PPh₃)₂ (Chart 1b).[16] Also, Buchner and coworkers carried out two reac-tions: beryllium dichloride in the presence of PMe₃ in benzene led to (PMe₃)₂BeCl₂ and beryllium dichloride reacted with bis(diphenylphosphino)propane in benzene to give the heterocyclic beryllium compound (CH₂)₃(Ph₂P)₂BeCl₂ (a six membered ring, Chart 1c).[17] Paparo and Jones made a ligand substitution in Et₂OBeX₂ (where X = Br, I) with diamines or diazabutadienes (DBAs) to prepare five-membered heterocyclic beryllium rings (Chart 1d).[18] The possibility of obtaining beryllium compounds without Be–halogen bonds was shown by Arrowsmith and Braunschweig in the synthesis of L₂Be (L = 1-(2,6-diisopropyl-phenyl)-3,3,5,5-tetramethylpyrrolidine-2-ylidene (CAAC), Chart 1e). First, they coordinated CAAC with the BeCl₂ in benzene, and then the second CAAC molecule was coordinated using KC₈ and EtO₂.[19] Paparo, Smith, and Jones carried out a reaction between BeBr₂(TMEDA) (TMEDA = *N*,*N*,*N'*,*N'*-tetramethylethylenediamine) and :Al(DIPNacNac) (DIPNacNac = (((2,6-diisopropylphenyl)NCMe)₂CH)⁻) in toluene, to get the first compound with a Be–Al bond (Chart 1f).[20] Puchta, Buchner, and co-workers synthesized

ᵃDepartamento de Química, Campus Guanajuato, Universidad de Guanajuato, Noria Alta S/N, CP 36050, Guanajuato, Gto, Mexico. E-mail: jjimenez@ugto.mx
ᵇInstitut de Química Computacional i Catàlisi and Departament de Química, Universitat de Girona, C/ Maria Aurèlia Capmany, 69, 17003 Girona, Catalonia, Spain. E-mail: miquel.sola@udg.edu
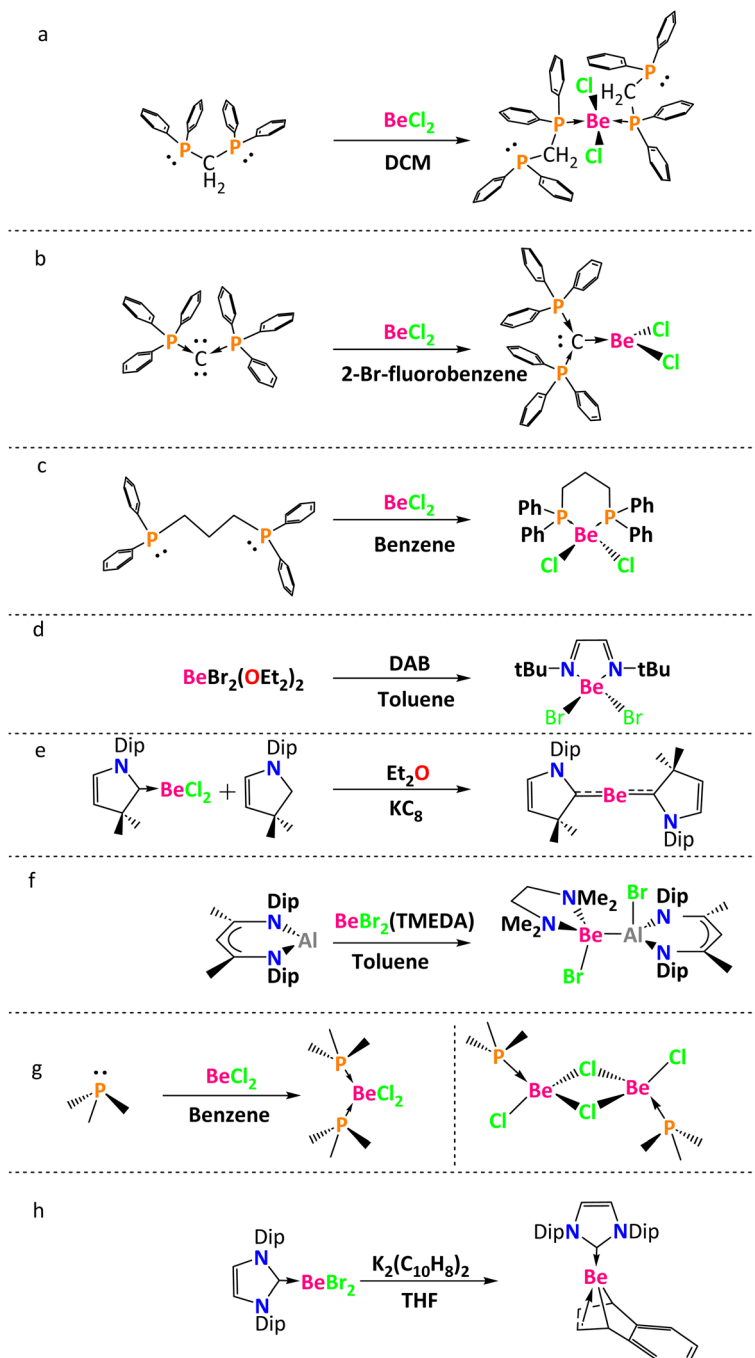†Electronic supplementary information (ESI) available. See DOI: https://doi.org/10.1039/d3dt02251j

Chart 1 Beryllium compounds reported with different ligands.

mono- and dinuclear beryllium halides $[(PMe_3)_2BeX_2]$ and $[(PMe_3)BeX_2]_2$, through the coordination of PMe_3 with the $BeCl_2$ in benzene (Chart 1g).[21] Finally, Paparo, Jones, and co-workers synthesized a beryllium naphthalenediyl complex through the reaction between $K_2(C_{10}H_8)_2(THF)$, that allowed the removal of the bromide ligands, and the stabilized NHC-BeBr$_2$ (Chart 1h).[22]

The importance of choosing an appropriate ligand is not only for better stabilization but also because beryllium compounds can activate bonds[23–25] and fixate small molecules.[26] Therefore, taking advantage of the preference of Be to form

bonds with halogens, we also aimed to tackle an environmental problem due to the use of phenyl halides (which are toxic, carcinogenic, and mutagenic).[27,28] On the other hand, aromatic halides are important in organic synthesis chemistry, but a limitation is found due to the inertness of the halogen–carbon bond.[29] Regarding the activation of C–X bonds, we can mention a series of examples provided by Matsubara and co-workers who carried out the amination of haloarenes using a nickel catalyst.[30] Also, Wu's group made fluorenes and polyarenes using 1-bromonaphthalene, diphenylethyne, and a palla-

dium catalyst.[31] Even, an alloy of palladium and gold carried out the C–Cl and C–Br bond activations (more reactive for Ar–Cl than Ar–Br).[32] Bickelhaupt, Hamlin, and co-workers studied the carbon(sp^n)–halogen bond activation using a Pd catalyst and found a decrement in the activation energies following the order C(sp^n)–F > C(sp^n)–Cl > C(sp^n)–Br > C(sp^n)–I.[33] Also, Harder and co-workers reported the hydrohalogenation of aromatic halides (with F, Cl, Br, and I) with alkaline-earth compounds (AeH, Ae = Ca, Sr, and Ba). They found that the conversion rate increases with the metal size (Ca < Sr < Ba) and halogen size (F < Cl < Br < I).[34]

Herein, using **(CAAC)$_2$Be**, **NtBuNtBuBe** (**NtBuNtBu** = (1E,2E)-N^1,N^2-di-$tert$-butylethane-1,2-diimine), **NNBe** (NN = (1E,2E)-N^1,N^2-dimethylethane-1,2-diimine), **NPBe** (NP = (1E,2E)-N-methyl-2-(methylphosphaneylidene)ethan-1-imine), **NOBe** (NO = (E)-2-(methylimino)acetaldehyde) and **NSBe** (NS = (E)-2-(methylimino)-ethanethial), we report on some plausible mechanistic proposals for the Ph–X (where X = F, Cl, Br, I) bond activation (see Scheme 1) and the effect of using mono- or bidentate ligands as Lewis bases to stabilize the empty orbitals of Be, adding an example of the ability of beryllium to act as other metals like Sr, Ca, Ba, Pd, and Ni. It is worth noting that among the different beryllium rings used, **NtBuNtBuBeBr$_2$** was prepared experimentally.[18] The **NtBuNtBuBe** species can be obtained by reduction of **NtBuNtBuBeBr$_2$** using solid potassium (*vide infra*).

Computational details

All DFT calculations were performed using the Gaussian09 program.[35] Geometries were optimized using Head-Gordon's hybrid functional that contains range-separated dispersion corrections (ωB97X-D).[36] The electronic configuration of the molecules was represented using the basis sets (def2-SVPP)

developed by Ahlrichs and co-workers.[37,38] The unrestricted formalism was used for the calculation of open-shell species. All the stationary points were classified according to their harmonic frequencies: only one imaginary frequency for transition states and positive values for all the frequencies for reactants, intermediates, and products. Gibbs energies were computed from the corrected electronic energies at the ωB97X-D/def2-TZVP(SMD:toluene)//ωB97X-D/def2-SVPP level obtained with the Gaussian09 program and including solvent effects with the solvation model based on solute electron density (SMD)[39] considering toluene as a solvent. Added corrections of the zero-point energy, thermal contributions to the internal energy, and the entropy term were computed at 298.15 K with the ωB97X-D/def2-SVPP method considering an ideal gas under standard conditions. For species **NNBe** and Ph–F, we performed additional calculations at the ωB97X-D/def2-TZVP (SMD:toluene)//ωB97X-D/def2-TZVP level of theory (see Fig. S7†). Differences in the energy profiles obtained by optimizing the geometries at the ωB97X-D/def2-SVPP or ωB97X-D/def2-TZVP level of theory are less than 1 kcal mol^{-1}, thus justifying the use of the ωB97X-D/def2-SVPP method for geometry optimizations. For a few elementary reaction steps, despite many attempts, we have been unable to locate the transition state (TS). In these cases, we have obtained an approximate relative electronic energy (ΔE) for the TS based on a linear transit that connects reactants and products. For these approximate TSs (marked with an asterisk in the reaction profiles), we provide the relative electronic energy obtained at the ωB97X-D/def2-TZVP(SMD:toluene)//ωB97X-D/def2-SVPP level. As they are not strict stationary points, Gibbs energies cannot be obtained with standard procedures.

Nucleus independent chemical shifts (NICS) were calculated at the B3PW91/6-311+G**//ωB97X-D/def2-SVPP level. Using the atomic partitioning obtained with the AIMALL program,[40] the multicenter indices (MCIs)[41–43] were computed
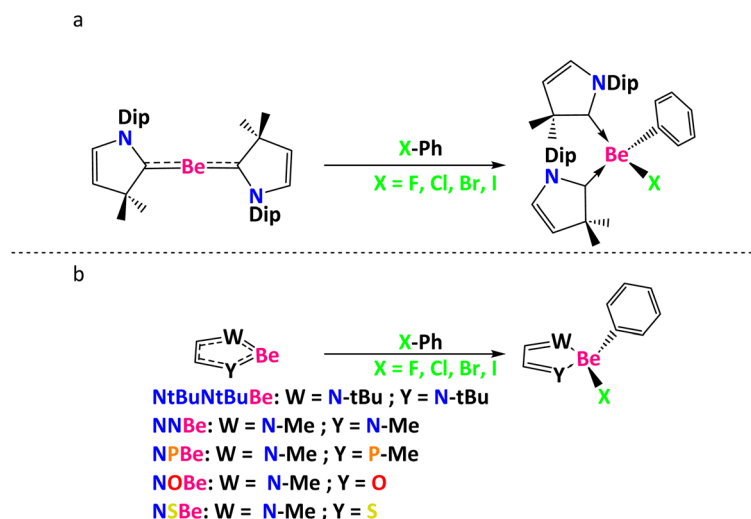
Scheme 1 C–X bond activations reported in this work (a) using **(CAAC)$_2$Be** and (b) using five-membered heterocyclic rings. Dip = 2,6-diisopropylphenyl.

with the ESI-3D[44–46] program at the ωB97X-D/def2-SVPP level. The wavefunction and the electronic structure were analyzed at the ωB97X-D/def2-TZVPP//ωB97X-D/def2-SVPP level of theory with the ORCA[47] and the IBOview[48] programs.

Using the ωB97X-D/def2-SVPP optimized geometries, energy decomposition analysis (EDA) was performed with the BLYP[49,50] functional and the TZ2P basis set with the Amsterdam density functional (ADF2019) software package.[51,52] The all-electron basis set used, denoted TZ2P, is of triple-ζ quality with two sets of polarization functions for all atoms. Standard convergence criteria and a fine grid were used. Dispersion forces were included *via* Grimme's dispersion correction scheme (DFT-D3(BJ)),[53] which contains the damping function proposed by Becke and Johnson.[54] In EDA, the interaction energy, ΔE_{int}, corresponds to the actual energy change when the geometrically deformed fragments are combined to form the overall complex. ΔE_{int} can further be decomposed within the framework of the canonical Kohn–Sham molecular orbital (MO) model.[55–59] The first term, ΔV_{elstat}, corresponds to the classical electrostatic interaction between the unperturbed charge distributions of the fragments in the geometry they possess in the complex. This term is usually attractive. The Pauli repulsion, ΔE_{Pauli}, between these fragments comprises the destabilizing interactions, associated with the Pauli principle for fermions, between occupied orbitals and is responsible for the steric repulsion. The orbital interaction, ΔE_{oi}, between these fragments in any MO model, and therefore also in Kohn–Sham theory, accounts for bond pair formation, charge transfer (empty/occupied orbital mixing between different fragments) and polarization (empty/occupied orbital mixing on one fragment due to the presence of another fragment). Finally, the ΔE_{disp} term accounts for attractive dispersion interactions.

Results and discussion

First, we carried out geometry optimizations for reactants (Fig. S1†). We tested different electronic configurations to find the ground state. **NtBuNtBuBe**, **NNBe**, **NPBe**, **NOBe**, and **NSBe** are closed-shell singlets, whereas **(CAAC)₂Be** is an open-shell broken symmetry singlet (the singlet closed-shell is higher in energy by 8.7 kcal mol^{-1}, see Table S1†).[60] For the **(CAAC)₂Be** complex, the Be–C distance is 1.646 Å (exp. 1.664 Å;[19] theor. 1.644 Å).[60] The Be–N bond lengths in all the rings vary from 1.516 to 1.536 Å (theor. 1.535 Å for **NNBe**[61]), while the P–Be, O–Be and S–Be bond lengths are 2.046, 1.464, and 2.046 Å, respectively. The C–C bond lengths oscillate from 1.354 to 1.360 Å and shorter C–C bond lengths are found when W and Y shown in Scheme 1 are different (see Fig. S1†).

The electronic structure for each ring was investigated with the IBOview program. The N, O, and S atoms tend to delocalize their electron pair inside the ring (to carbon and beryllium atoms) while P does not share its lone pair (see Fig. 1). Other works reported five-membered rings with a non-planar phosphine moiety.[62,63] Using effective oxidation states (EOSs) defined by Salvador *et al.*,[64] we determined that the EOS of the Be atom is 2+ at all stationary points that were located (also in **(CAAC)₂Be**). We also carried out EDA for the **NNBe** taking Be as one of the fragments and the ligand as the other one. We considered the Be fragment in different oxidation and spin states: Be^0 (singlet and triplet), Be^{1+} (doublet) as reported by Parameswaran's group for a similar compound, BeN₂(CH₃)₂C₂H₂,[61] and Be^{2+} (singlet). Taking the oxidation state from the lowest stabilizing ΔE_{oi} value,[65,66] we also found that the oxidation state of Be is 2+ (see Fig. S2†). This agrees with the intrinsic bond orbitals (IBOs) displayed in Fig. 1 that indicate that Be does not have a lone pair.
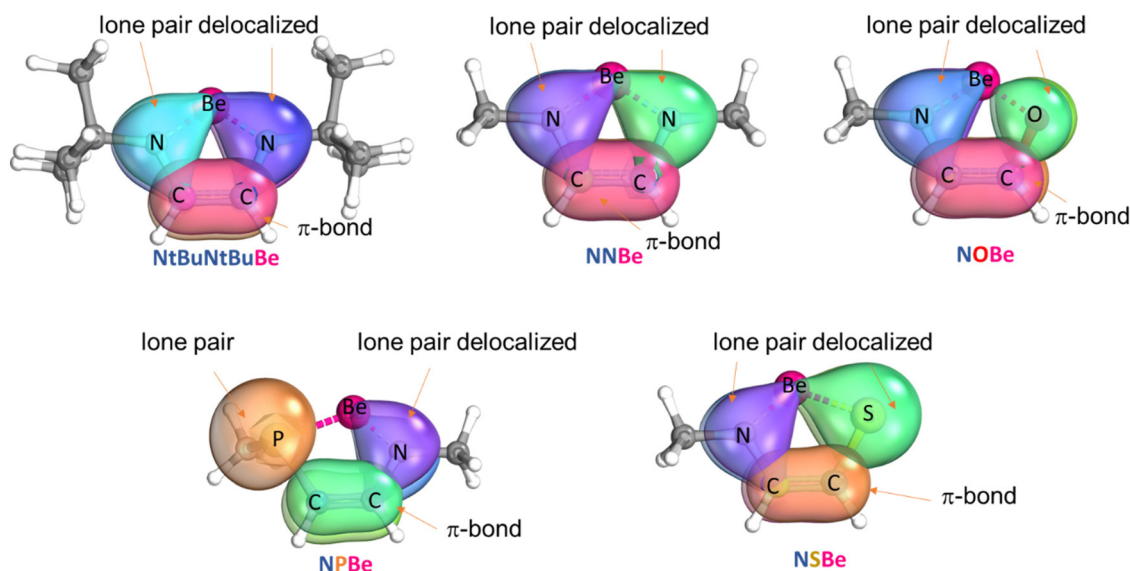

Fig. 1   IBOs for heterocyclic beryllium compounds.

Due to the electron delocalization, we considered the possibility of these compounds to have an aromatic character (rings with formally 6π-electrons); we calculated the NICS index at the B3PW91/6-311+G**//ωB97X-D/def2-SVPP level of theory. In accordance with our results, the NICS(0) values are −8.3 (benzene), −9.2 (**N***t***BuN***t***BuBe**), −8.7 (**NNBe**), −8.0 (**NSBe**), −6.3 (**NOBe**) and −2.9 (**NPBe**) ppm. All of the rings except **NPBe** show relatively large negative values that indicate the aromatic character of these rings with six π-electrons[61,67] (for NICS(1)$_{zz}$ values, see Table S2†). In the **NPBe** system, the phosphorus electron pair is not involved in the π-system, which quenches the aromaticity of this ring. Our NICS result of **NNBe** agrees with that reported by Parameswaran's group (NICS$_{zz}$(1) = −9.6).[61] The aromatic character of the rings, indicated by NICS results, is further substantiated by the MCI values (see Table S2†). From the computed normalized MCI values (MCI$^{1/n}$)[68] we obtained the following order of aromaticity: benzene (0.59) > **NNBe** (0.51) ≈ **N***t***BuN***t***BuBe** (0.50) ≈ **NOBe** (0.50) ≈ **NSBe** (0.50) > **NPBe** (0.47), which agrees with the NICS ordering. On the other hand, the isomerization stabilization energies (ISEs)[69] provide a different order of aromaticity, that is, **NSBe** > **NPBe** > **NOBe** > **NNBe**, and prove that the aromatic stabilization energy of these systems is relatively low (Table S4†).[70]

Before starting with the activation of the Ph–X bonds, we calculated the reduction of **N***t***BuN***t***BuBeBr$_2$** using a K$_{10}$ cluster of C_s symmetry[71] to get **N***t***BuN***t***BuBe**, two molecules of KBr, and a K$_8$ cluster of C_{2v} symmetry (Scheme 2).[71] The Gibbs reaction energy is clearly favorable according to our calculations (ΔG(SMD = toluene) = −43.4 kcal mol^{-1}). Thus, we now discuss the reaction mechanism for the halogen–carbon bond activation using the **N***t***BuN***t***BuBe** ring (Fig. 2).

The reaction starts with the donor–acceptor interaction between one of the lone pairs of the halogen and the LUMO of **N***t***BuN***t***BuBe** (**1.1a**, Fig. 2) that is mainly located on the Be atom.[61] This step is exergonic for F but not for Cl, Br, and I. Through the transition state (TS) **1.2a**, that describes the Ph–X bond cleavage with $\Delta G^{\ddagger}$ = 27.2 (F), 27.0 (Cl), 22.9 (Br), and 21.6 (I) kcal mol^{-1}, we got **1.3a** (the process is kinetically more favorable in the following order: I > Br > F ∼ Cl). Intermediate **1.3a** is characterized by a tetracoordinate beryllium compound with a 2+ oxidation state of Be. Next, the phenyl group migrates from Be to N (TS **1.4a** with $\Delta G^{\ddagger}$ = 21.3 (F), 24.1 (Cl), 25.2 (Br), and 27.8 (I) kcal mol^{-1}) to get the product **1.5a**. According to EOS, Be does not change the oxidation state of 2+ along the reaction. The electron density needed for the bond
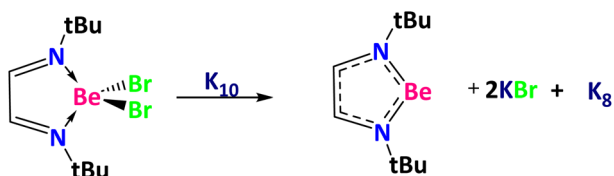
activation comes from the ligand that plays a non-innocent role (*vide infra*).

The Gibbs reaction energy is exergonic for all halogens, with the exergonicity decreasing as the halogen becomes heavier. Except for I, the Gibbs energy barriers to generate product **1.5a** from **1.3a** are lower in energy than those of the **1.1a** → **1.3a** process. The TOF-determining intermediate (TDI)[72] is **1.1a** for F or reactants for Cl and Br and the TOF-determining transition state (TDTS) is **1.2a** for F, Cl, and Br, whereas for I the TDI is **1.3a** and the TDTS is **1.4a**. The energetic span (TDTS–TDI energy difference) values are 27.2 (F), 27.0 (Cl), 22.9 (Br), and 27.8 (I) kcal mol^{-1}. According to our results, the most favorable activation takes place for Ph–Br. Fig. S5† shows other reaction paths that were analyzed for this **N***t***BuN***t***BuBe** system but were ruled out because they were found to be higher in energy than those presented in Fig. 2.

The second reaction mechanism that we have studied corresponds to the **NNBe** ring (Fig. 3). As before, the reaction starts with the halogen coordination with the Be moiety in an exergonic process. This interaction is more favorable in **NNBe** than in **N***t***BuN***t***BuBe** because in the latter the LUMO is located higher in energy by about 0.11 eV.

To get **2.3a** (favorable for all halogens in the order F > Br > Cl > I), it is necessary to surmount the TS **2.2a** corresponding to the bond activation with $\Delta G^{\ddagger}$ = 23.6 (F), 20.6 (Cl), 17.2 (Br), and 15.6 (I) kcal mol^{-1}. The lower barriers for **NNBe** than those for **N***t***BuN***t***BuBe** are attributed to the higher steric hindrance of the TS **1.2a** in the **N***t***BuN***t***BuBe** species. For the **NNBe** compound, we carried out an IBO analysis along the reaction coordinate for the Ph–F bond activation (Fig. S4†). In **NNBe**-FPh (**2.1a**), the ring redistributes electron density from the C–C π bond to the antibonding Ph–F and results in **2.3a** (Fig. S4a†). In this way, the Be atom does not change its oxidation state. It is the ligand that promotes the oxidative addition of Ph–F by becoming oxidized. The ligand participates in the redox process as a redox non-innocent ligand that behaves as an electron reservoir.[73,74] During the process, the ligand loses its aromaticity (see Table S2†).

Through the TS **2.4a**, which corresponds to the phenyl group migration from Be to N (with $\Delta G^{\ddagger}$ = 18.5 (F), 22.1 (Cl), 23.0 (Br), and 24.6 (I) kcal mol^{-1}), we got the final product **2.5a**. The reaction energies are more exergonic for F than for Cl, Br, and I. To pass from **2.3a** to **2.5a**, the N–C π bond donates electron density to the Be–Ph σ* antibonding orbital that, as a result, is weakened, favoring the formation of the N–Ph bond (Fig. S4b†).

The energetic spans, which are determined by the intermediate **2.1a** and the TS **2.2a** for F and the intermediate **2.3a** and the TS **2.4a** for Cl, Br, and I, are 23.6 (F), 22.1 (Cl), 23.0 (Br), and 24.6 (I). The change of the substituent *t*Bu by Me favors the reaction by decreasing the Gibbs energy barriers and increasing the exergonicity of the reaction.

The next mechanism is for the **NPBe** reaction (Fig. 4). In an exergonic step the reaction starts with the formation of the intermediate **3.1a** (favorable in the following order: I > F > Cl > Br). Through the TS **3.2a**, that corresponds to the oxidative
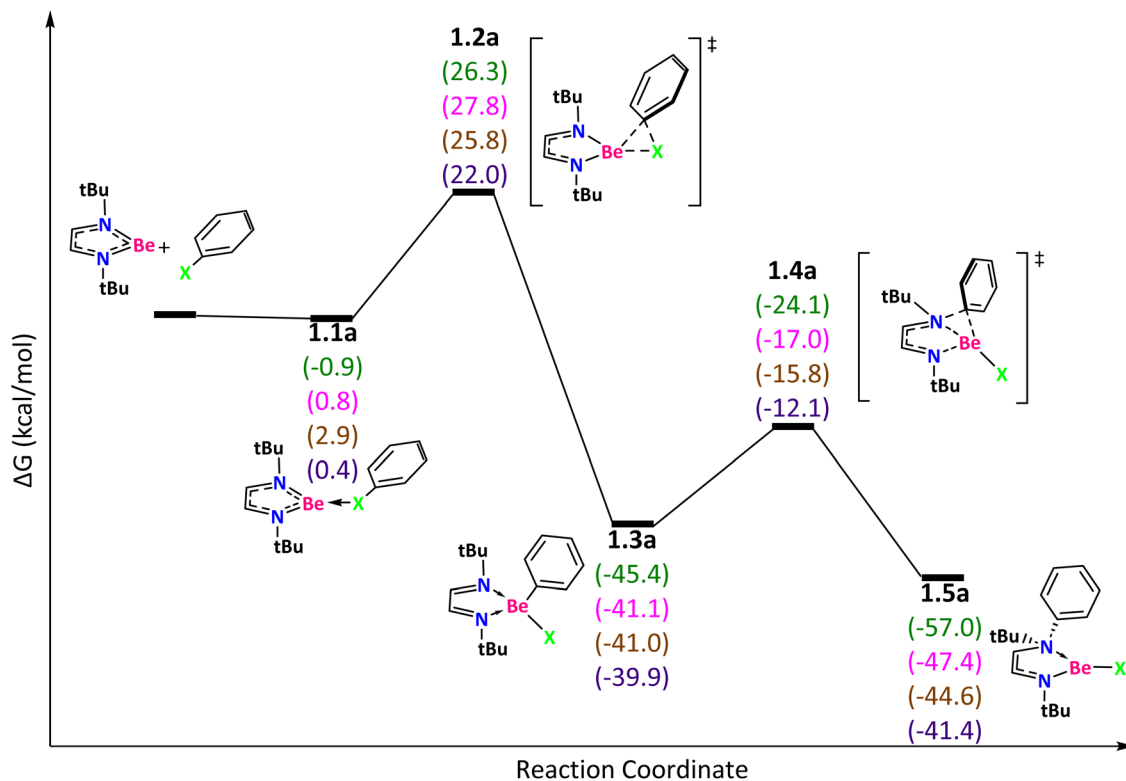

Scheme 2 N*t*BuN*t*BuBeBr$_2$ reduction to N*t*BuN*t*BuBe.

Fig. 2 Reaction mechanism determined at the ωB97X-D/def2-TZVP(SMD:toluene)//ωB97X-D/def2-SVPP level. X = F (green), Cl (pink), Br (brown), and I (purple).

Fig. 3 Reaction mechanism determined at the ωB97X-D/def2-TZVP(SMD:toluene)//ωB97X-D/def2-SVPP level. X = F (green), Cl (pink), Br (brown), and I (purple).

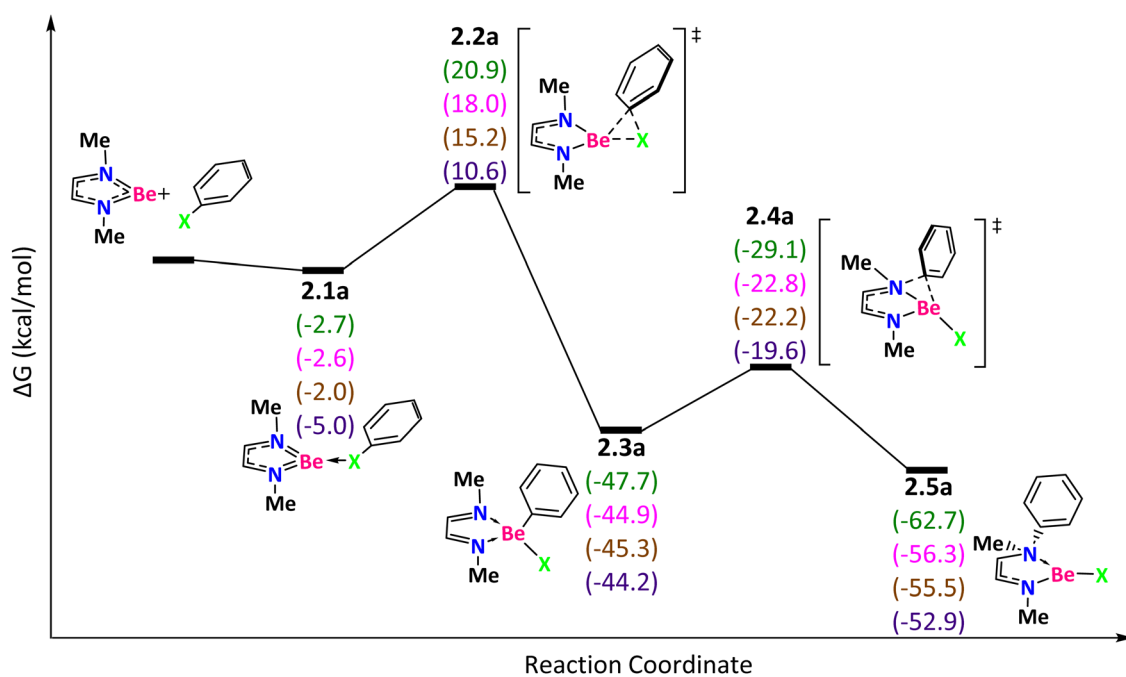**Fig. 4** Reaction mechanism determined at the ωB97X-D/def2-TZVP(SMD:toluene)//ωB97X-D/def2-SVPP level. X = F (green), Cl (pink), Br (brown), and I (purple).

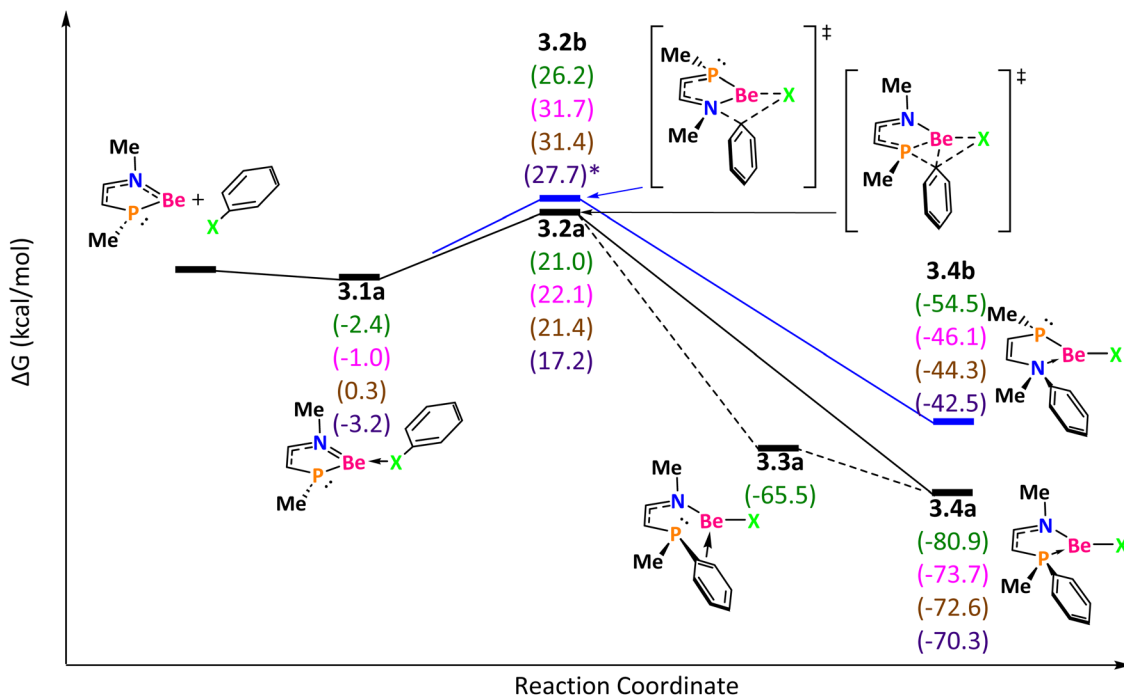addition of the Ph–X bond (with $\Delta G^{\ddagger}$ = 23.4 (F), 23.1 (Cl), 21.4 (Br) and 20.4 (I) kcal mol^{-1}), we got the product **3.4a** (except for F, for which after the TS we got **3.3a** and then **3.4a** in a barrierless process). An alternative pathway involves crossing the TS **3.2b** that describes the phenyl group migration from the halogen to nitrogen (with $\Delta G^{\ddagger}$ = 28.6 (F), 32.7 (Cl), and 31.4 (Br) and $\Delta E^{\ddagger}$ of 25.3 (F), 31.1 (Cl), 43.0 (Br) and 43.3 (I) kcal mol^{-1}), through which we got the product **3.4b**. The difference between **3.4a** and **3.4b** is the position of the phenyl group, on P or N, respectively. The Gibbs reaction energies are favorable in both cases but it is more for **3.4a** than for **3.4.b** (in the two reactions the exergonicity follows the order: F > Cl > Br > I). The reason for the higher stability of **3.4a** than that of **3.4b** is attributed to the greater capability of the phosphine group to share electron density in comparison to that of the amine (phosphorus is softer and less electronegative than nitrogen).[75] Also, the delocalization of the N electron pair over the ring stabilizes the product while the electron pair of P cannot be delocalized.

When Y contains an element of group 16 (O or S), we found additional paths that are not present in the reaction mechanisms discussed above. For **NOBe** (Fig. 5), the reaction starts with an exergonic step to form **4.1a**, favorable in the following order: I > F > Br ~ Cl. If the reaction proceeds through the TS **4.2a**, with $\Delta G^{\ddagger}$ = 25.2 (F) ($\Delta E^{\ddagger}$ = 24.0 (F), 9.1 (Cl), 9.5 (Br), and 14.0 (I) kcal mol^{-1}), the phenyl group migrates from the halogen to N and the product **4.5a** is obtained. We have explored alternative pathways but all of them were found to be higher in energy. For instance, if the reaction goes through the TS **4.2b**, the phenyl group migrates from the halogen to O to

generate **4.5b** with $\Delta G^{\ddagger}$ = 29.9 (F) ($\Delta E^{\ddagger}$ = 29.8 (F), 23.2 (Cl), 25.6 (Br), and 30.2 (I) kcal mol^{-1}). Now, if the reaction passes through the TS **4.2c**, with $\Delta G^{\ddagger}$ = 24.0 (Cl), 20.8 (Br), and 18.5 (I) kcal mol^{-1} ($\Delta E^{\ddagger}$ = 27.6 (F), 24.0 (Cl), 20.5 (Br), 18.9 (I) kcal mol^{-1}), the phenyl group migrates from the halogen to Be producing the tetracoordinate beryllium compound **4.3c** with the following exergonicity order: F > Cl > Br > I. From that intermediate, if the phenyl group migrates from Be to N (the TS **4.4c** with $\Delta G^{\ddagger}$ = 10.4 (F), 12.2 (Cl), 12.4 (Br), and 13.7 (I) kcal mol^{-1}), the product is **4.5a**. The other TS **4.4d** (with $\Delta G^{\ddagger}$ = 22.1 (F), 24.2 (Cl), 24.6 (Br) and 25.9 (I) kcal mol^{-1}), that describes the phenyl group migration from Be to O, leads to the product **4.5b**. The product **4.5a** is thermodynamically more stable than **4.5b**. In conclusion, the expected main product for all halogens is **4.5a** obtained by surmounting the TS **4.2a**.

For the last bidentate ligand, **NSBe** (Fig. 6), the reaction starts with an exergonic step to form **5.1a**, favorable in the following order: I > F > Cl > Br. If the reaction passes through the TS **5.2a**, with $\Delta G^{\ddagger}$ = 29.2 (F) and 32.8 (Cl) ($\Delta E^{\ddagger}$ = 27.6 (F), 30.7 (Cl), 14.8 (Br), and 17.4 (I) kcal mol^{-1}), the phenyl group migrates from the halogen to N and the product **5.5a** is obtained. If the reaction goes through the TS **5.2b**, with $\Delta G^{\ddagger}$ = 29.7 (F) ($\Delta E^{\ddagger}$ = 29.4 (F), 24.2 (Cl), 21.5 (Br) and 21.8 (I) kcal mol^{-1}), the phenyl group migrates from the halogen to S and the product **5.5b** is generated. Now, if the reaction passes through TS **5.2c**, with $\Delta G^{\ddagger}$ = 30.6 (Cl), 26.6 (Br) and 25.1 (I) kcal mol^{-1}, the phenyl group migrates from the halogen to Be and the tetracoordinate beryllium compound **5.3c** is produced with the following exergonicity order: Cl > Br > I. In the case of F, all the attempts to locate **5.2c** ended in **5.2a**. Therefore, we
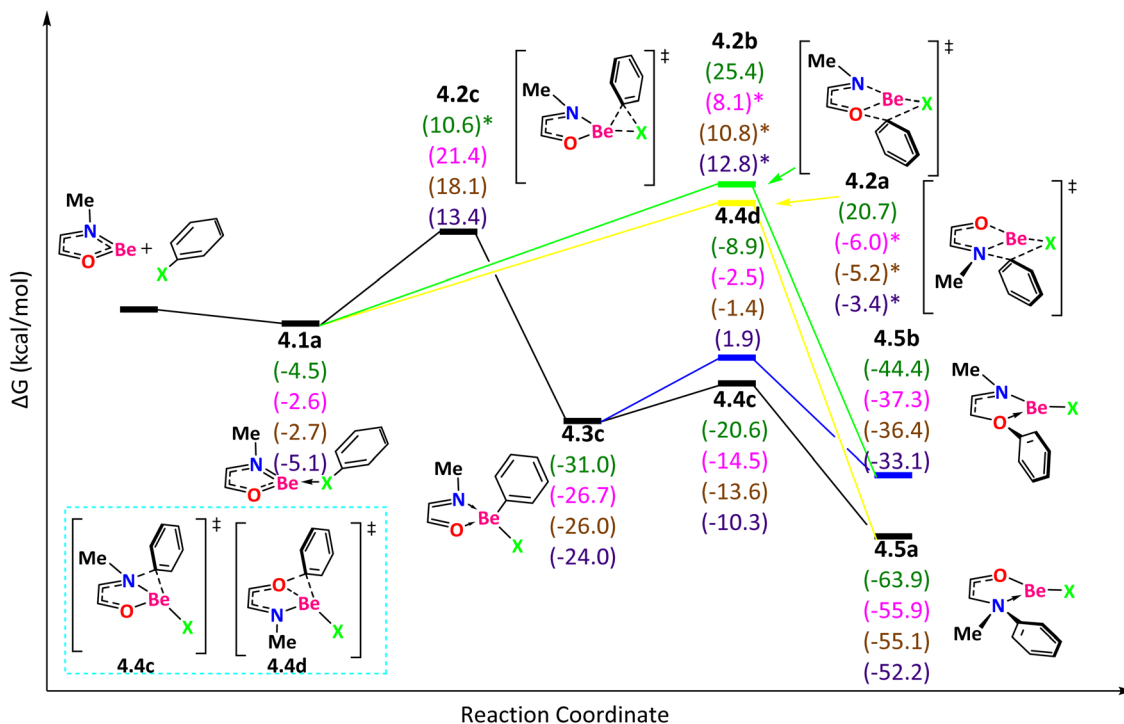
Fig. 5 Reaction mechanism determined at the ωB97X-D/def2-TZVP(SMD:toluene)//ωB97X-D/def2-SVPP level. X = F (green), Cl (pink), Br (brown), and I (purple).
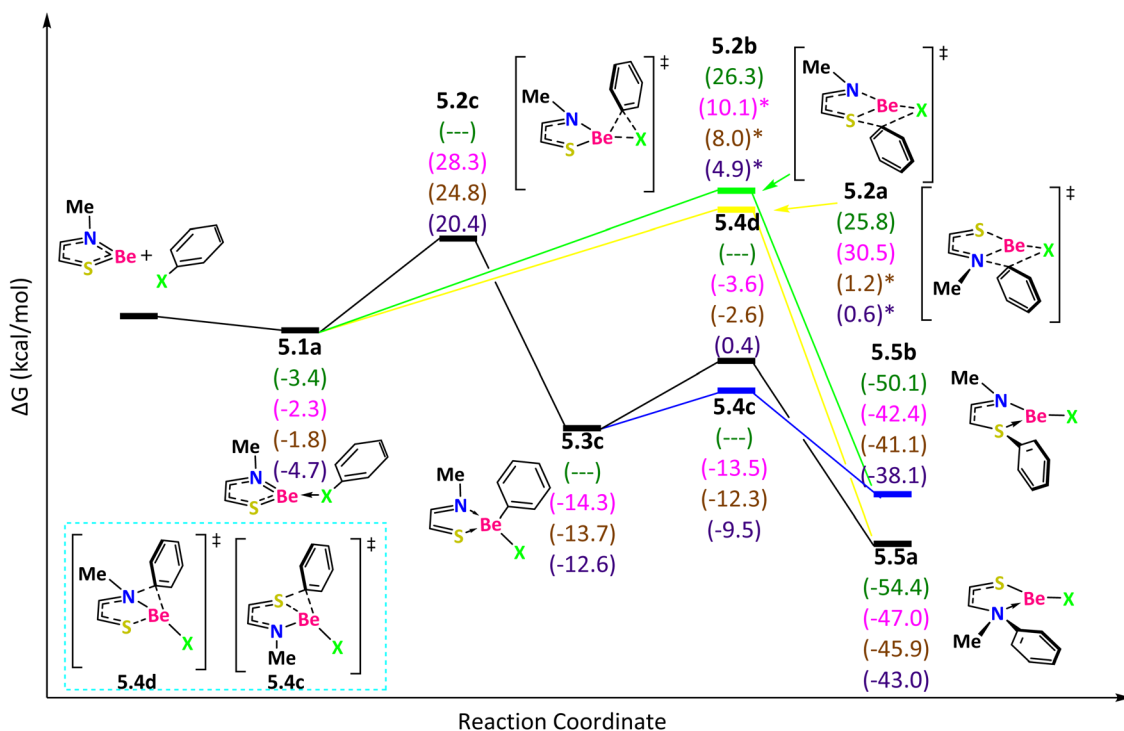

Fig. 6 Reaction mechanism determined at the ωB97X-D/def2-TZVP(SMD:toluene)//ωB97X-D/def2-SVPP level. F (green), Cl (pink), Br (brown), and I (purple). The dashed lines indicate that no intermediate or TS exists for that halogen.

conclude that the route through **5.2c** is not possible for Ph–F activation. From the intermediate **5.3c**, if the phenyl group migrates from Be to N (TS **5.4d** with $\Delta G^{\ddagger} = 10.7$ (Cl), 11.1 (Br) and 13.0 (I) kcal mol^{-1}), the product is **5.5a**. The other TS **5.4c** (with $\Delta G^{\ddagger} = 0.8$ (Cl), 1.4 (Br) and 3.1 (I) kcal mol^{-1}), that describes the phenyl group migration from Be to S, leads to the product **5.5b**. The product **5.5a** is more favorable than **5.5b**.

In all cases, during the first step corresponding to the oxidative addition, the aromaticity of the five-membered heterocyclic ring is lost (Table S2†). As said before, the loss of aromatic stabilization energy when going from reactants to **x.2a** is higher in **NSBe** (11.9 kcal mol^{-1}) than in **NOBe** (5.7 kcal mol^{-1}) or **NNBe** (3.8 kcal mol^{-1}). Interestingly, for systems with similar steric hindrance such as **NSBE**, **NOBe** and **NNBe**, the five-membered heterocyclic rings with higher aromatic stabilization energy in the reactant are those having the larger Gibbs energy barriers for the oxidative addition (Table S4†), as expected from the fact that during the oxidative addition the five-membered heterocyclic ring loses its aromaticity.

In general, when the TS describes the Ph–X bond activation (where Ph is bonded to Be, N, P, O, or S), the activation energy is highest for X = F and it is due to the higher strength of the Ph–F bond (see Table S3†). The higher the Ph–X bonding energy, the higher the energy barrier is. For the same reason (stronger Be–F bonds), usually the case X = F provides the most exergonic processes (see Table S3†). Other reaction paths involving bicyclic intermediates were tested but they were found to be highly endergonic and they were not further analyzed (Fig. S5†).

Finally, the **(CAAC)₂Be** system was studied (Fig. 7). The reaction starts with a concerted transition state that describes the Ph–X bond activation with $\Delta G^{\ddagger} = 49.2$ (F), 53.4 (Cl), 53.2 (Br) and 53.0 (I) kcal mol^{-1}. We found high Gibbs energy barriers in this process despite lack of aromaticity in **(CAAC)₂Be**. These high energy barriers are due to the fact that the **(CAAC)₂Be** system must deform significantly by decreasing the ∠CBeC angle to provide space for the interaction of the LUMO of **(CAAC)₂Be** with the HOMO of the Ph–X molecule (Fig. S6†). The deformation energy values are 14.1 (F), 15.1 (Cl), 15.7 (Br), and 16.7 (I) kcal mol^{-1}. Once **6.1a** is surmounted, formation of **6.2a** is highly exergonic with $\Delta G^{\ddagger} = 14.9$ (F), 16.3 (Cl), 16.9 (Br) and 17.1 (I) kcal mol^{-1} (**6.3a**), and the phenyl group in **6.2a** migrates from the Be to the carbenic carbon to generate **6.4a**. The Gibbs reaction energies are exergonic in the following order: F > Cl > Br > I.

Conclusions

The reaction mechanisms of the phenyl–halogen bond activation using beryllium compounds were studied. The analysed
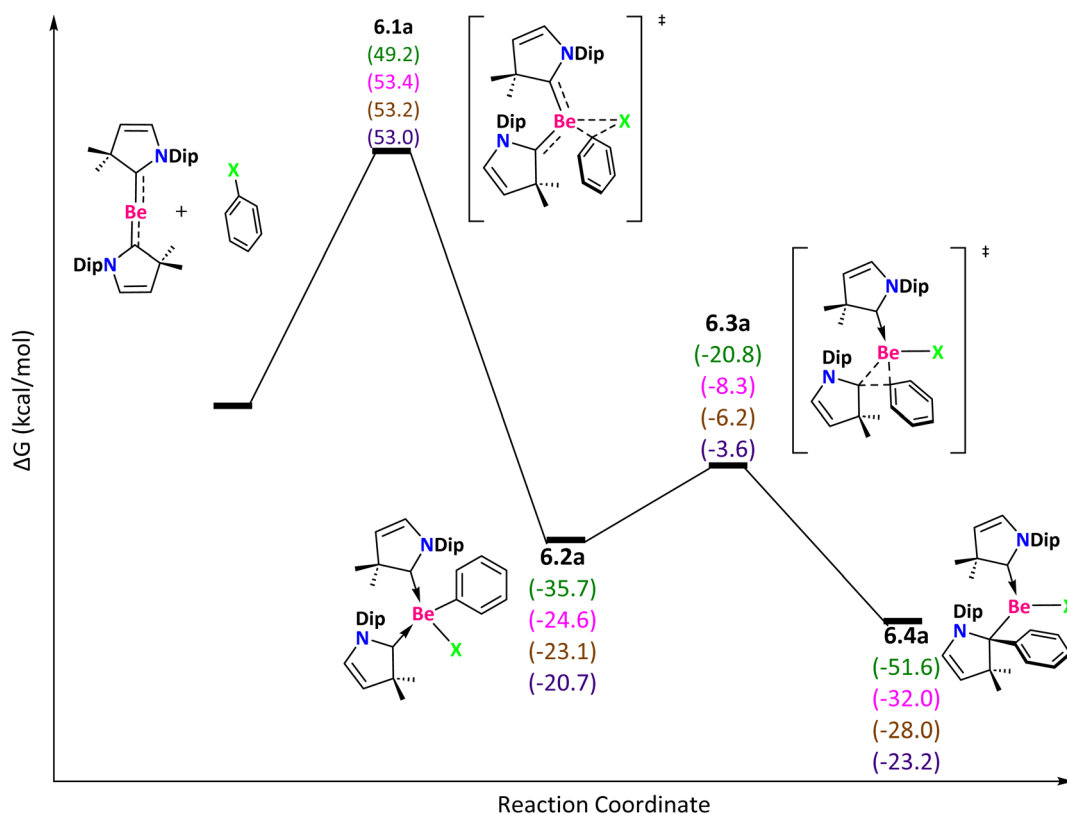

Fig. 7 Reaction mechanism determined at the ωB97X-D/def2-TZVP(SMD:toluene)//ωB97X-D/def2-SVPP level. X = F (green), Cl (pink), Br (brown), and I (purple).

beryllium five-membered rings have a closed-shell singlet ground state, whereas the **(CAAC)₂Be** species has an open-shell singlet as the ground state. The beryllium five-membered ring exhibits aromaticity due to the delocalization of electrons in the cycle. According to the energy profiles, the activation of Ph–X bonds involves exergonic reactions, favorable in the following order: **NPBe > NNBe > NOBe > N*t*BuN*t*BuBe > NSBe > CAAC₂Be**, as the halogen becomes heavier. In many cases, the rate determining step is the oxidative addition that occurs in the first step of the reaction. In general, the higher the aromatic stabilization energy of the five-membered heterocyclic ring, the greater the energy barrier for the oxidative addition. This process also benefits from the reduction of the steric hindrance of the compounds. Interestingly, Be(ɪɪ) retains the oxidation state along the whole reaction path and the electrons needed for the oxidative addition are given by the ligands that have a key role in the reaction. In this sense, the metallomimetic character of the beryllium complexes is more provided by the ligands than by the element itself. For the **(CAAC)₂Be** species, the Gibbs energy barriers are high because of the need to distort the reactants to allow the interaction with the Ph–X species.

Data availability

The data that support the findings of this study are available in the ESI† of this article.

Conflicts of interest

The authors declare no conflict of interest.

Acknowledgements

References

1 M. R. Buchner and L. R. Thomas-Hargreaves, *Dalton Trans.*, 2021, **50**, 16916–16922.
2 P. P. Power, *Nature*, 2010, **463**, 171–177.
3 C. Weetman, *Chem. – Eur. J.*, 2021, **27**, 1941–1954.
4 M.-A. Légaré, C. Pranckevicius and H. Braunschweig, *Chem. Rev.*, 2019, **119**, 8231–8261.
5 M. S. Hill, D. J. Liptrot and C. Weetman, *Chem. Soc. Rev.*, 2016, **45**, 972–988.
6 K. A. Walsh and E. E. Vidal, *Beryllium Chemistry and Processing*, ASM International, Materials Park, Ohio, 2009.
7 R. Puchta, *Nat. Chem.*, 2011, **3**, 416–416.
8 M. R. Buchner, *Chem. – Eur. J.*, 2019, **25**, 12018–12036.
9 *Beryllium: Mineralogy, Petrology, and Geochemistry*, ed. E. S. Grew, Mineralogical Society Of America, Washington, DC, 2002.
10 D. Naglav, M. R. Buchner, G. Bendt, F. Kraus and S. Schulz, *Angew. Chem., Int. Ed.*, 2016, **55**, 10562–10576.
11 K. J. Iversen, S. A. Couchman, D. J. D. Wilson and J. L. Dutton, *Coord. Chem. Rev.*, 2015, **297**, 40–48.
12 J. L. Dutton and G. Frenking, *Angew. Chem., Int. Ed.*, 2016, **55**, 13380–13382.
13 P. Parameswaran and G. Frenking, *J. Phys. Chem. A*, 2010, **114**, 8529–8535.
14 D. E. Trujillo-González, G. González–García, T. A. Hamlin, F. M. Bickelhaupt, H. Braunschweig, J. O. C. Jiménez–Halla and M. Solà, *Eur. J. Inorg. Chem.*, 2023, **26**, e202200767.
15 G. Frenking, N. Holzmann, B. Neumüller and K. Dehnicke, *Z. Anorg. Allg. Chem.*, 2010, **636**, 1772–1775.
16 W. Petz, K. Dehnicke, N. Holzmann, G. Frenking and B. Neumüller, *Z. Anorg. Allg. Chem.*, 2011, **637**, 1702–1710.
17 M. R. Buchner, M. Müller and S. S. Rudel, *Angew. Chem., Int. Ed.*, 2017, **56**, 1130–1134.
18 A. Paparo and C. Jones, *Chem. – Asian J.*, 2019, **14**, 486–490.
19 M. Arrowsmith, H. Braunschweig, M. A. Celik, T. Dellermann, R. D. Dewhurst, W. C. Ewing, K. Hammond, T. Kramer, I. Krummenacher, J. Mies, K. Radacki and J. K. Schuster, *Nat. Chem.*, 2016, **8**, 890–894.
20 A. Paparo, C. D. Smith and C. Jones, *Angew. Chem., Int. Ed.*, 2019, **58**, 11459–11463.
21 M. R. Buchner, D. Ćоćić, S. I. Ivlev, N. Spang, M. Müller and R. Puchta, *Dalton Trans.*, 2023, **52**, 5287–5296.
22 A. Paparo, A. J. R. Matthews, C. D. Smith, A. J. Edwards, K. Yuvaraj and C. Jones, *Dalton Trans.*, 2021, **50**, 7604–7609.
23 M. Arrowsmith, M. S. Hill, G. Kociok-Köhn, D. J. MacDougall and M. F. Mahon, *Angew. Chem., Int. Ed.*, 2012, **51**, 2098–2100.
24 M. R. Buchner, N. Spang, M. Müller and S. S. Rudel, *Inorg. Chem.*, 2018, **57**, 11314–11317.
25 K. G. Pearce, M. S. Hill and M. F. Mahon, *Chem. Commun.*, 2023, **59**, 1453–1456.
26 T. J. Hadlington and T. Szilvási, *Nat. Commun.*, 2022, **13**, 461.
27 M. A. Keane, *Appl. Catal., A*, 2004, **271**, 109–118.
28 K. V. Murthy, P. M. Patterson and M. A. Keane, *J. Mol. Catal. A: Chem.*, 2005, **225**, 149–160.
29 V. V. Grushin and H. Alper, *Chem. Rev.*, 1994, **94**, 1047–1062.
30 K. Matsubara, K. Ueno, Y. Koga and K. Hara, *J. Org. Chem.*, 2007, **72**, 5069–5076.
31 C.-W. Lee, E.-C. Liu and Y.-T. Wu, *J. Org. Chem.*, 2015, **80**, 10446–10456.

32 R. N. Dhital, K. Bobuatong, M. Ehara and H. Sakurai, *Chem. – Asian J.*, 2015, **10**, 2669–2676.

33 B. P. Moloto, P. Vermeeren, M. Dalla Tiezza, C. Esterhuysen, F. M. Bickelhaupt and T. A. Hamlin, *Eur. J. Org. Chem.*, 2022, e202200722.

34 M. Wiesinger, B. Rösch, C. Knüpfer, J. Mai, J. Langer and S. Harder, *Eur. J. Inorg. Chem.*, 2021, **2021**, 3731–3741.

35 M. J. Frisch, G. W. Trucks, H. B. Schlegel, G. E. Scuseria, M. A. Robb, J. R. Cheeseman, G. Scalmani, V. Barone, G. A. Petersson, H. Nakatsuji, X. Li, M. Caricato, A. Marenich, J. Bloino, B. G. Janesko, R. Gomperts, B. Mennucci, H. P. Hratchian, J. V. Ortiz, A. F. Izmaylov, J. L. Sonnenberg, D. Williams-Young, F. Ding, F. Lipparini, F. Egidi, J. Goings, B. Peng, A. Petrone, T. Henderson, D. Ranasinghe, V. G. Zakrzewski, J. Gao, N. Rega, G. Zheng, W. Liang, M. Hada, M. Ehara, K. Toyota, R. Fukuda, J. Hasegawa, M. Ishida, T. Nakajima, Y. Honda, O. Kitao, H. Nakai, T. Vreven, K. Throssell, J. A. Montgomery Jr., J. E. Peralta, F. Ogliaro, M. Bearpark, J. J. Heyd, E. Brothers, K. N. Kudin, V. N. Staroverov, T. Keith, R. Kobayashi, J. Normand, K. Raghavachari, A. Rendell, J. C. Burant, S. S. Iyengar, J. Tomasi, M. Cossi, J. M. Millam, M. Klene, C. Adamo, R. Cammi, J. W. Ochterski, R. L. Martin, K. Morokuma, O. Farkas, J. B. Foresman and D. J. Fox, *Gaussian 09, Revision D.01*, Gaussian, Inc., Wallingford CT, 2016.

36 J.-D. Chai and M. Head-Gordon, *J. Chem. Phys.*, 2008, **128**, 084106.

37 F. Weigend and R. Ahlrichs, *Phys. Chem. Chem. Phys.*, 2005, **7**, 3297.

38 F. Weigend, *Phys. Chem. Chem. Phys.*, 2006, **8**, 1057.

39 A. V. Marenich, C. J. Cramer and D. G. Truhlar, *J. Phys. Chem. B*, 2009, **113**, 6378–6396.

40 T. A. Keith, *AIMAll (Version 19.10.12), TK Gristmill Software*, Overland Park KS, USA, 2019 (https://aim.tkgristmill.com).

41 M. Giambiagi, M. Segre De Giambiagi, C. D. Dos Santos Silva and A. Paiva De Figueiredo, *Phys. Chem. Chem. Phys.*, 2000, **2**, 3381–3392.

42 P. Bultinck, R. Ponec and S. Van Damme, *J. Phys. Org. Chem.*, 2005, **18**, 706–718.

43 F. Feixas, E. Matito, J. Poater and M. Solà, *Chem. Soc. Rev.*, 2015, **44**, 6434–6451.

44 E. Matito, M. Solà, P. Salvador and M. Duran, *Faraday Discuss.*, 2007, **135**, 325–345.

45 E. Matito, M. Duran and M. Solà, *J. Chem. Phys.*, 2005, **122**, 014109; Erratum, *ibid.*, 2005, **125**, 059901.

46 E. Matito, *ESI-3D: Electron Sharing Indices Program for 3D Molecular Space Partitioning*, Institute of Computational chemistry and Catalysis (IQCC), University of Girona, Catalonia, Spain, 2006; https://iqcc.udg.es/~eduard/ESI (accessed 12th July 2023).

47 F. Neese, F. Wennmohs, U. Becker and C. Riplinger, *J. Chem. Phys.*, 2020, **152**, 224108.

48 G. Knizia, *J. Chem. Theory Comput.*, 2013, **9**, 4834–4843.

49 A. D. Becke, *Phys. Rev. A*, 1988, **38**, 3098–3100.

50 C. Lee, W. Yang and R. G. Parr, *Phys. Rev. B: Condens. Matter Mater. Phys.*, 1988, **37**, 785–789.

51 G. te Velde, F. M. Bickelhaupt, E. J. Baerends, C. Fonseca Guerra, S. J. A. van Gisbergen, J. G. Snijders and T. Ziegler, *J. Comput. Chem.*, 2001, **22**, 931–967.

52 C. Fonseca Guerra, J. G. Snijders, G. te Velde and E. J. Baerends, *Theor. Chem. Acc.*, 1998, **99**, 391–403.

53 S. Grimme, J. Antony, S. Ehrlich and H. Krieg, *J. Chem. Phys.*, 2010, **132**, 154104.

54 E. R. Johnson and A. D. Becke, *J. Phys. Chem.*, 2005, **123**, 024101.

55 P. Vermeeren, S. C. C. van der Lubbe, C. Fonseca Guerra, F. M. Bickelhaupt and T. A. Hamlin, *Nat. Protoc.*, 2020, **15**, 649–667.

56 M. Bickelhaupt, *J. Comput. Chem.*, 1999, **20**, 114–128.

57 W.-J. van Zeist and F. M. Bickelhaupt, *Org. Biomol. Chem.*, 2010, **8**, 3118.

58 F. M. Bickelhaupt and E. J. Baerends, in *Kohn-Sham Density Functional Theory: Predicting and Understanding Chemistry*, ed. K. B. Lipkowitz and D. B. Boyd, Wiley-VCH, New York, 1999, pp. 199–212.

59 T. A. Hamlin, P. Vermeeren, C. Fonseca Guerra and F. M. Bickelhaupt, in *Complementary Bonding Analysis*, ed. S. Grabowsky, De Gruyter, 2021, pp. 199–212.

60 M. Gimferrer, S. Danés, E. Vos, C. B. Yildiz, I. Corral, A. Jana, P. Salvador and D. M. Andrada, *Chem. Sci.*, 2022, **13**, 6583–6591.

61 S. Parambath, J. Narayanan S. J. and P. Parameswaran, *Dalton Trans.*, 2023, **52**, 3378–3385.

62 H. Jacobsen, *J. Organomet. Chem.*, 2005, **690**, 6068–6078.

63 W. W. Schoeller and D. Eisner, *Inorg. Chem.*, 2004, **43**, 2585–2589.

64 E. Ramos-Cordoba, V. Postils and P. Salvador, *J. Chem. Theory Comput.*, 2015, **11**, 1501–1508.

65 C. R. Landis, R. P. Hughes and F. Weinhold, *Organometallics*, 2015, **34**, 3442–3449.

66 P. Jerabek, P. Schwerdtfeger and G. Frenking, *J. Comput. Chem.*, 2019, **40**, 247–264.

67 M. Solà, A. I. Boldyrev, M. K. Cyrański, T. M. Krygowski and G. Merino, *Aromaticity and Antiaromaticity: Concepts and Applications*, John Wiley & Sons, Ltd, Chichester, West Sussex, 2023.

68 J. Cioslowski, E. Matito and M. Solà, *J. Phys. Chem. A*, 2007, **111**, 6521–6525.

69 P. V. R. Schleyer and F. Pühlhofer, *Org. Lett.*, 2002, **4**, 2873–2876.

70 M. K. Cyrański, *Chem. Rev.*, 2005, **105**, 3773–3811.

71 S. Abdalla, M. Springborg and Y. Dong, *Surf. Sci.*, 2013, **608**, 255–264.

72 S. Kozuch and S. Shaik, *Acc. Chem. Res.*, 2011, **44**, 101–110.

73 V. Lyaskovskyy and B. De Bruin, *ACS Catal.*, 2012, **2**, 270–279.

74 L. A. Berben, B. De Bruin and A. F. Heyduk, *Chem. Commun.*, 2015, **51**, 1553–1554.

75 H. Anane, S. El Houssame, A. El Guerraze, A. Jarid, A. Boutalib, I. Nebot-Gil and F. Tomás, *J. Mol. Struct. (THEOCHEM)*, 2004, **709**, 103–107.